REGULAR ARTICLE

Atoms in molecules: beyond Born–Oppenheimer paradigm

Mohammad Goli · Shant Shahbazian

Abstract This contribution presents the first *atoms in molecules* study that goes beyond the Born–Oppenheimer paradigm employing the newly developed two-component quantum theory of atoms in molecules (TC-QTAIM). The LiH, LiD, and LiT systems containing quantum instead of clamped hydrogen nuclei are used as typical examples. The computational analysis that is done on non-adiabatic wavefunctions derived from the fully variational multi-component molecular orbital approach (FV-MC-MO) results in hydrogen atomic basins without any clamped nucleus. The topological analysis of the Γ-field, the field that replaces the usual one-electron density used in the orthodox topological analysis, reveals delicate differences among the considered systems. The calculation of basin properties also demonstrates that the TC-QTAIM differentiates among atomic basins containing isotopes. Since the nuclear dynamics is contained intrinsically in non-adiabatic wavefunctions, the nuclear contribution to both topological analysis and basin properties naturally emerges from the TC-QTAIM analysis resolving the long-standing obstacle of consistent incorporation of nuclear dynamics within the context of the orthodox QTAIM. Also, a similar analysis is done on non-adiabatic wavefunctions describing excited instead of ground nuclear vibrations of the considered systems demonstrating the fact that TC-QTAIM is capable of being employed for both ground and excited nuclear vibrational states.

M. Goli · S. Shahbazian (✉)
Department of Chemistry, Faculty of Sciences,
Shahid Beheshti University, G. C., Evin, Tehran, Iran
e-mail: chemist_shant@yahoo.com

1 Introduction

There is no doubt that the Born–Oppenheimer separation of electronic and nuclear dynamics is one of the cornerstones of modern theoretical chemistry setting the stage for introducing most of the modern computational quantum chemistry by validating the celebrated clamped nuclei model (CNM) as a reasonable approximation [1, 2]. It has also a pivotal role in developing many useful concepts routinely used in theoretical chemistry [3–8]. However, in contrast to its general success, it is a well-known fact that for lightest nuclei, this approximation must be abandoned at least for certain applications invoking a theoretically sounder picture. Indeed, in recent years, a renaissance has been taken place in the so-called non-Born–Oppenheimer (non-BO) calculations discarding the CNM from the *outset* and treating protons and other light particles on an equal footing with electrons as genuine quantum waves [9–20]. The non-BO calculations reveal certain features like charge asymmetry in isotopically substituted diatomics [21–24], tunneling effect in hydrogen transfer [25–27], isotope-dependent phase transition temperature of hydrogen bonded ferroelectrics [28], as well as various other delicate isotope effects [29–35] that are not generally derivable from computational procedures developed within the context of the CNM. The quantum treatment of nuclei may have also interesting impacts on the analysis of molecular structure and chemical bonding by not only incorporating the quantum dynamics of nuclei in bonding analysis, but also directly verifying the role of isotope substitution on

structure and bonding [36–40]. Accordingly, inspired by the recent formulation of the Quantum Theory of Atoms in Positronic Molecules (QTAIP) [41–43], an Atoms in Molecules (AIM) approach is here introduced that aims at discriminating hydrogen atoms and their properties beyond the CNM. It is demonstrated that not only this novel approach is capable of incorporating the quantum nature of hydrogen nuclei into the AIM framework, but also it distinguishes delicate differences between hydrogen atomic basins containing proton, deuterium, and tritium nuclei. The effect of nuclear vibrational excitations on the AIM approach is also considered demonstrating that the proposed AIM is sensitive enough to reveal nuclear vibration effect on the properties of bonded hydrogen atoms.

2 A brief summary of basic theory and computational procedure

The QTAIP is the extension of the Quantum Theory of Atoms in Molecules (QTAIM) [44–46] to the positronic species. However, the basic formulation of the QTAIP is independent from the nature of positron and may easily be used for electronic systems containing extra positively charged quantum particles like protons, deuterons, tritiums. Thus, this basic formalism may be called as the Two-Component Quantum Theory of Atoms in Molecules (TC-QTAIM); electronic systems composed of electrons and a type of positively charged quantum particles with an arbitrary mass (this formalism reduced to the QTAIP by setting $m_+ = m_{positron}$). Instead of the μ-field of the QTAIP, the following mass-weighted field called Γ-field is introduced based on one-particle densities [41–43].

$$\Gamma(q) = \rho_-(q) + \gamma \rho_+(q)$$
$$\gamma = m_-/m_+, \quad \rho_\pm(q) = N_\pm \int d\tau' \Psi^* \Psi \tag{1}$$

In these equations, minus subscripts denote electronic properties, whereas plus subscripts refer to the properties of positively charged quantum particles (m_- and m_+ are the masses of electron and positively charged particle, respectively). Also, $d\tau'$ denotes the sum over spin variables of all quantum particles and integration over all spatial coordinates except for a single electron or positively charged particle designated through the subscript. The zero-flux surfaces of the Γ-field, surfaces emerging from $\vec{\nabla}\Gamma(q) \cdot \vec{n} = 0$ ($\vec{n}$ is the unit vector normal to the surface), delineate the boundaries of the *topological atoms*; the latter consist of the global attractors of the Γ-field and their associated basins [43]. The resulting atomic basins not only have a well-defined regional kinetic energy but also the regional viral theorem is valid for these regions [41, 42]

(In a recent paper [47], Ayers and coworkers have rigorously demonstrated that apart from the so-called Laplacian family of the local kinetic energy densities [48, 49] that are associated with the general family of $\vec{\vec{\sigma}}_{\alpha,\beta}(\vec{r})$ stress tensor densities, there are also other possible families of local kinetic energy density. In this as well as previous studies, it is assumed that all local mechanical properties are associated with Schrödinger-Pauli-Epstein stress tensor density, $\vec{\vec{\sigma}}_{0.5,0}(\vec{r})$ in Ayer's nomenclature [47], so no ambiguity emerges). Each regional observable is defined and calculated from the two-component regional hypervirial theorem that takes the contribution of all quantum particles into account [43].

For the purpose of computational implementation of the proposed AIM analysis, the code previously developed for positronic species [42] was further extended to deal with the Γ-field and associated regional properties. Moreover, the 3D views of atomic basins were constructed employing the AIM2000 package [50–52]. The non-BO wavefunctions of the LiH system as well as those of its isotopomers, LiD and LiT, were constructed using the fully variational multicomponent molecular orbital approach (FV-MC-MO) developed by Tachikawa and coworkers [9, 10]. In these calculations, the hydrogen nuclei are considered as quantum waves like electrons, whereas the Li nucleus is modeled as a clamped nucleus; the used masses of proton, deuteron, and tritium are those advocated for by Nakatsuji and coworkers [19]. The s-type Gaussian basis functions were used for expanding ground state wavefunctions for both electronic and nuclear functions; these are denoted as [6s:1s], [6s:2s], and [6s:3s] sets employing the nomenclature proposed by Sherrill and coworkers [14]. All variables of these functions including their centers, exponents, and expansion coefficients were then fully optimized simultaneously. The machinery of our FV-MC-MO code and its optimization strategy will be disclosed elsewhere. The results of calculations gathered in supporting information, Tables S1–S4, not only conform well with a previous study on these systems [53], but also demonstrate that [6s:1s] combination is flexible enough for the subsequent AIM analysis. Also, since the wavefunctions are fully optimized, the virial ratio is very close to its exact value, $-\langle V \rangle / \langle T \rangle = 2$, Table S4, and no virial scaling is needed in order to compute the regional energies of atomic basins [42]. In order to model the first excited vibrational state of these species, a [6s:1p$_z$] combination was used to prevent the "variational collapse" to the ground vibrational state. The computed energy spacing of the ground and first excited vibrational state of LiH ($\sim$4,202–4,205 cm^{-1} by the three basis sets), Table S5, is in reasonable agreement with that reported by Sherrill and coworkers at the CIS computational level ($\sim$4,108 cm^{-1}) demonstrating the

reliability of our excited state calculations [14]. Throughout this paper, all quantities are presented in the usual atomic units (au) unless otherwise stated.

3 Results and discussion

3.1 Topological analysis

The AIM analysis starts from the topological analysis of the Γ, ρ_-, and ρ_+ fields of LiX ($X = H, D, T$) systems [42]. Figure 1 depicts typical relief maps of these fields, whereas Figs. S1 and S2 depict the relevant contour maps. Also, Table 1 presents several quantitative results from the topological analysis. It is evident from these figures that

Γ and ρ_- are quite similar, each containing two $(3, -3)$ and one $(3, -1)$ critical points (CPs), though, the quantitative differences are also apparent from Table 1. As is evident from Figs. 1 and S1, this similarity is not surprising since ρ_+ is concentrated around its corresponding $(3, -3)$ CP (located at ~ 3.2 au away from the Li nucleus), and its contribution to Γ is scaled by $\gamma \prec 0.001$. For a fine quantitative picture of the distribution of ρ_+, the population of positively charged particle was integrated within hypothetical spheres with centers at the $(3, -3)$ CP of the ρ_+-fields. The results presented in Table S6 demonstrate that almost all of the proton, deuteron, and tritium populations are located inside spheres with radius ~ 0.7, ~ 0.6, and ~ 0.5 au, respectively. Beyond this radius, the amount of ρ_+ is negligible, and thus, they are called the Effective

Fig. 1 Typical relief maps of the Γ, ρ_- (*top*), and ρ_+ (*bottom*) for the systems considered at FV-MC-MO/[6s:1s] level. The Li clamped nucleus is located at $(0, 0)$ point
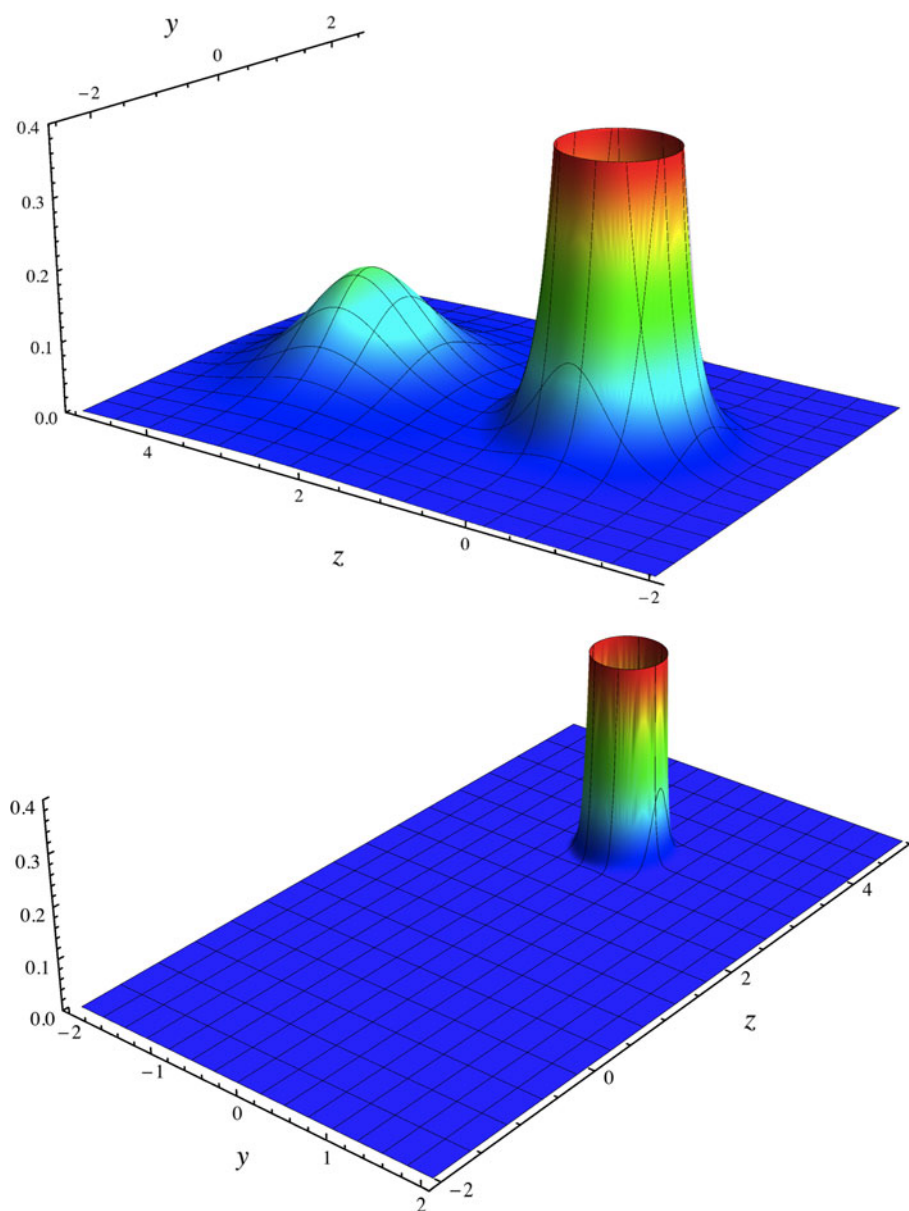
Table 1 The results of topological analysis performed on the ground state of LiH, LiD, LiT, as well as LiH(∞) (clamped hydrogen nucleus)

	Γ			ρ_+ $(3, -3)$	ρ_-		
	Li	BCP	$(3, -3)$		Li	BCP	$(3, -3)$
LiH							
Field	11.437	0.027	0.182	36.211	11.437	0.027	0.163
Field Lap.	−3,524.024	0.145	−5.121	−7,470.997	−3,524.024	0.145	−1.133
Hess.	−1,174.676	−0.033	−1.719	−2,490.332	−1,174.676	−0.033	−0.378
Com.	−1,174.672	0.211	−1.684	−2,490.332	−1,174.672	0.211	−0.376
Dis. (3, −3)[a]	0.000	1.398	3.184	3.202	0.000	1.398	3.119
G	0.001	0.032	0.004	0.000	0.001	0.032	0.000
K	881.007	−0.004	1.285	1,867.749	881.007	−0.004	0.283
V	−881.009	−0.028	−1.289	−1,867.749	−881.007	−0.028	−0.283
LiD							
Field	11.436	0.028	0.186	63.513	11.436	0.028	0.170
Field Lap.	−3,522.383	0.147	−6.321	−19,057.584	−3,522.383	0.147	−1.232
Hess.	−1,174.129	−0.034	−2.122	−6,352.528	−1,174.129	−0.034	−0.412
Com.	−1,174.125	0.214	−2.078	−6,352.528	−1,174.125	0.214	−0.409
Dis. (3, −3)[a]	0.000	1.395	3.170	3.185	0.000	1.395	3.107
G	0.001	0.033	0.005	0.000	0.001	0.033	0.000
K	880.597	−0.004	1.586	4,764.396	880.597	−0.004	0.308
V	−880.598	−0.028	−1.591	−4,764.396	−880.598	−0.028	−0.308
LiT							
Field	11.435	0.028	0.188	87.668	11.435	0.028	0.173
Field Lap.	−3,521.021	0.148	−7.094	−32,611.511	−3,521.021	0.148	−1.280
Hess.	−1,173.675	−0.034	−2.381	−10,870.504	−1,173.675	−0.034	−0.427
Com.	−1,173.671	0.216	−2.332	−10,870.504	−1,173.671	−0.216	−0.425
Dis. (3, −3)[a]	0.000	1.393	3.165	3.178	0.000	1.393	3.102
G	0.001	0.033	0.006	0.000	0.001	0.033	0.000
K	880.257	−0.004	1.780	8,152.878	880.257	−0.004	0.320
V	−880.258	−0.029	−1.786	−8,152.878	−880.258	−0.029	−0.320
LiH(∞)[b]							
Field	–	–	–	–	11.433	0.029	0.189
Field Lap.	–	–	–	–	−3,517.774	0.151	−1.522
Hess.	–	–	–	–	−1,172.593	−0.035	−0.508
Com.	–	–	–	–	−1,172.589	0.222	−0.506
Dis. Li	–	–	–	–	0.000	1.386	3.077
Dis. H	–	–	–	–	3.077	1.691	0.000
G	–	–	–	–	0.002	0.034	0.000
K	–	–	–	–	879.445	−0.004	0.381
V	–	–	–	–	−879.447	−0.029	−0.381

Field entry denotes the amount of Γ, ρ-fields, whereas Lap. is an abbreviation for the Laplacian operator. Hess. Com. are the three components of the diagonalized Hessian matrix. The first entry in each case is the degenerate component of the Hessian matrix. dis. is the acronym of "distance from". The G, K, and V are used to denote the Lagrangian, Hamiltonian, and total virial fields. See references [41] and [42] for details and definitions. All values are presented in the atomic units

[a] Distance from the (3, −3) CP located very near to Li nucleus

[b] In this case, a fully variational [6s:1s] basis set is used to construct the wavefunction assuming $m_+ = 1.00E + 13$ au. The validity of this calculation was verified independently by comparing with a fully variational [6s] (only electronic basis set) calculation within the CNM context

Size of nucleus Distribution (ESD). Although this means that the ρ_+ contributes directly to Γ only in a limited region of space within the ESD, its indirect influence namely the *polarization* and *accumulation* of ρ_- field is significant as is clear from Figs. 1 and S2. On the other hand, the regular contraction of the ESD from proton to tritium is in line with

the fact that a heavier quantum particle is more localized than a lighter one.

If one uses various topological indexes at the Bond Critical Point (BCP) of Γ, the $(3, -1)$ CP, $\tilde{M}(q) = M_+(q) + M_-(q)$ [42, 43], as indicators of chemical bonding, it is evident that the gross features of bonding are quite similar in these species and all are similar to that derived within the context of the CNM, LiH(∞), Table 1; all indicating a predominantly ionic bonding [44–46]. However, a detailed comparison of the topological indexes in the four considered systems reveals delicate differences and demonstrates that they are not completely equal. Particularly, the position of the $(3, -1)$ CP (BCP) shifts slightly toward the Li nucleus as one goes from LiH to LiT and then LiH(∞). Since this point is part of the zero-flux surface that acts as the interatomic boundary surface, one may conclude that the *geometry* of the atomic boundaries and consequently the atomic basins themselves are not the same in these systems; shrinking toward the Li nucleus by the increase in the mass of the positively charged particle. Consequently, this indicates that the TC-QTAIM differentiates among atomic basins of isotopically substituted topological atoms. By comparing the center and the radius of the ESD with the position of the BCP in each

of considered species in Table 1, it emerges that $\Gamma^{BCP} \approx \rho_-^{BCP}\left(\rho_+^{BCP} \approx 0\right)$. In line with previous discussions, this demonstrates that the direct contribution of nuclear distribution to the topological indexes of BCPs is negligible, and the differences among the topological indexes of these species originate from varied *polarization* of ρ_- by ρ_+, the nuclear distribution; the fingerprint of the latter on ρ_- is unique since it is regulated by the nucleus mass.

3.2 Atomic basins and their properties

The second stage in the AIM analysis is the delineation of atomic basins and their properties [41–43]. Figure 2 depicts typical atomic basins, and Table 2 presents some of their properties, $\int_\Omega dq\tilde{M}(q) = M(\Omega)$, as well as those of the clamped nucleus congener [42, 43]. In order to check the integration accuracy, the net flux integral of each atomic basin, $\tilde{L}(\Omega) = (-1/4)\int_\Omega dq\nabla^2\Gamma(q)$, in addition to the sum of basin properties, total energies, and electric dipole moments, are considered at first [42]. The former is null in a successful basin integration $(\tilde{L}(\Omega) = 0)$, whereas the latter must be equal to the ab initio calculated total properties of the considered species, $(M_{total} = \sum_\Omega M(\Omega))$ [42].

Fig. 2 (*top*) The molecular volume encompassed by an isodensity surface ($\Gamma = 0.01$ au) containing three dots that are the two $(3, -3)$ CPs and the single BCP of Γ-field. The hydrogen atom is on the *right-hand side,* whereas the lithium atom is located on the *left-hand side* of this panel. (*bottom*) The two atomic basins depicted separately with different magnifications. The hydrogen's basin is depicted in the *left panel,* whereas lithium's is in the *right panel.* The *red dots* are the BCP in both panels
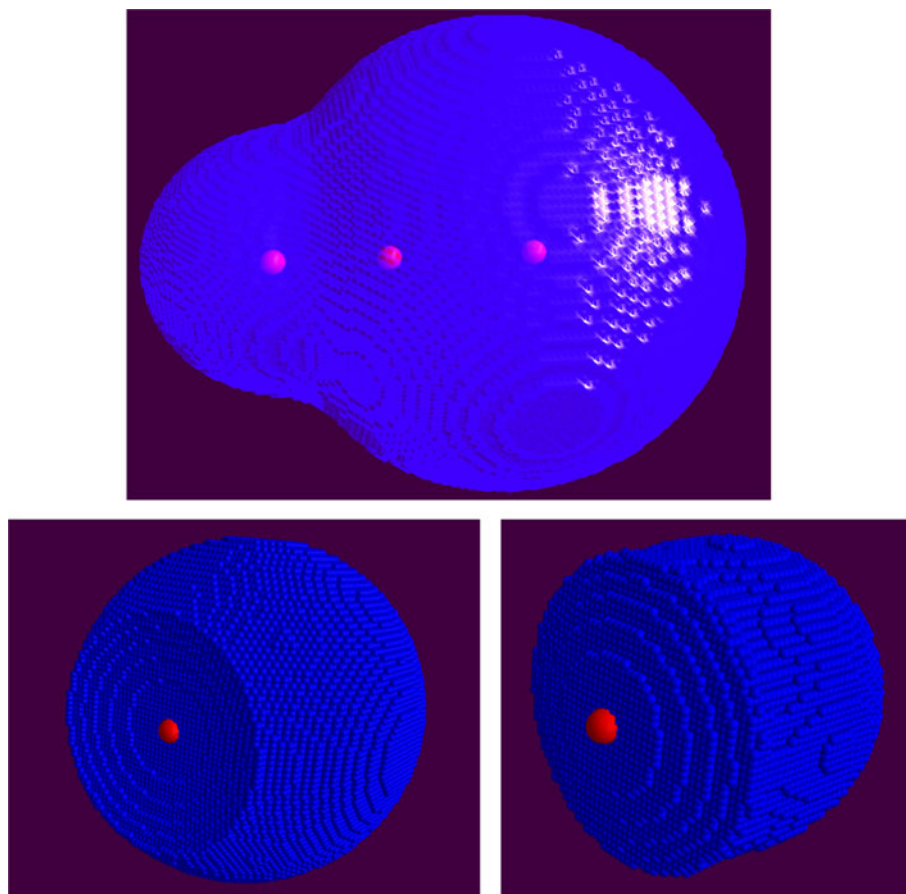
Table 2 The results of the basin integrations performed on LiH, LiD, LiT, as well as LiH(∞)

Molecule/property	Atoms			Molecule/property	Atoms		
	Li	X	Sum		Li	X	Sum
LiH				*LiD*			
Energy	−7.34309	−0.57080	−7.91389	Energy	−7.34301	−0.57921	−7.92223
Electronic charge	0.91388	−0.91388	0.00000	Electronic charge	0.91506	−0.91506	0.00000
Kinetic energy (*G*)	7.34310	0.57080	7.91389	Kinetic energy (*G*)	7.34302	0.57921	7.92223
Kinetic energy (*K*)	7.34310	0.57080	7.91390	Kinetic energy (*K*)	7.34303	0.57921	7.92224
Total virial (*V*)	−14.68620	−1.14160	−15.82780	Total virial (*V*)	−14.68605	−1.15842	−15.84447
Net flux int.	0.000003	0.000005	–	Net flux int.	0.000003	0.000005	–
Ele. energy	−7.34309	−0.55675	−7.89984	Ele. energy	−7.34301	−0.56900	−7.91201
Nuc. energy	0.00000	−0.01405	−0.01405	Nuc. energy	0.00000	−0.01022	−0.01022
CT ele. dipole	0.00000	−6.09281	−6.09281	CT ele. dipole	0.00000	−6.07122	−6.07122
CT nuc. dipole	0.00000	3.20169	3.20169	CT nuc. dipole	0.00000	3.18539	3.18539
First ele. moment	0.00307	0.41955	0.42263	First ele. moment	0.00219	0.41337	0.41557
First nuc. moment	0.00000	0.00000	0.00000	First nuc. moment	0.00000	0.00000	0.00000
Total ele. dipole	0.00307	−5.67326	−5.67018	Total ele. dipole	0.00219	−5.65785	−5.65566
Total nuc. dipole	0.00000	3.20169	3.20169	Total nuc. dipole	0.00000	3.18539	3.18539
Total dipole	0.00307	−2.47156	−2.46849	Total dipole	0.00219	−2.47246	−2.47027
LiT				*LiH(∞)*			
Energy	−7.34299	−0.58300	−7.92599	Energy	−7.34287	−0.60054	−7.94341
Electronic charge	0.91559	−0.91559	0.00000	Electronic charge	0.91788	−0.91788	0.00000
Kinetic energy (*G*)	7.34298	0.58299	7.92597	Kinetic energy (*G*)	7.34289	0.60054	7.94344
Kinetic energy (*K*)	7.34298	0.58300	7.92598	Kinetic energy (*K*)	7.34290	0.60055	7.94344
Total virial (*V*)	−14.68596	−1.16599	−15.85195	Total virial (*V*)	−14.68579	−1.20109	−15.88688
Net flux int.	0.000003	0.000005	–	Net flux int.	0.000002	0.000004	–
Ele. energy	−7.34299	−0.57454	−7.91753	Ele. energy	−7.34287	−0.60054	−7.94341
Nuc. energy	0.00000	−0.00846	−0.00846	Nuc. energy	0.00000	0.00000	0.00000
CT ele. dipole	0.00000	−6.06200	−6.06200	CT ele. dipole	0.00000	−2.88659	−2.88659
CT nuc. dipole	0.00000	3.17821	3.17821	CT nuc. dipole	0.00000	0.00000	0.00000
First ele. moment	0.00182	0.41098	0.41280	First ele. moment	0.00034	0.41390	0.41424
First nuc. moment	0.00000	0.00000	0.00000	First nuc. moment	0.00000	0.00000	0.00000
Total ele. dipole	0.00182	−5.65102	−5.64920	Total ele. dipole	0.00034	−2.47269	−2.47235
Total nuc. dipole	0.00000	3.17821	3.17821	Total nuc. dipole	0.00000	0.00000	0.00000
Total dipole	0.00182	−2.47281	−2.47098	Total dipole	0.00034	−2.47269	−2.47235

The int., ele., and nuc. are abbreviations for integral, electronic, and nuclear, respectively. See references [41] and [42] for details and definitions. All values are presented in the atomic units

As is evident from Tables 2 and S4, both of these criteria are satisfied within the usual accepted numerical accuracy [44–46].

A comparison of basin energies reveals the fact that within the bounds of the chemical accuracy (~ 0.001 Hartree or ~ 1 kcal mol^{-1}), the energy of lithium basins is the same for the four considered systems. In contrast, the energies of hydrogen basins are diminished by the increase in the mass of nucleus and the differences span well beyond the chemical accuracy (~ 19 kcal mol^{-1} from LiH

to LiH(∞)). Since the energy of the total system is the summation of the lithium and hydrogen basins, this quantity also diminishes by the increase in the mass of the quantum nucleus. On the other hand, the energy of the hydrogen basin in contrast to the lithium basin is composed of electronic and nuclear contributions, $\tilde{E}(\Omega) = E_{+}(\Omega) + E_{-}(\Omega)$ [42]; as it is expected, the nuclear contribution originating from the nuclear vibrations diminishes by increasing the nuclear mass but its contribution to the total energy of the hydrogen atomic basins of LiH, LiD, and LiT

is quite well beyond the chemical accuracy, ~ 8.8, ~ 6.4, and ~ 5.3 kcal mol^{-1}, respectively. In order to compare with zero-point vibrational energies, following the proposed recipe of Tachikawa and coworkers [54], the optimized exponents of nuclear s-type Gaussian basis functions were used to derive the harmonic vibrational frequencies. These are 4,107.3, 2,988.3, and 2,473.7 cm^{-1} for LiH, LiD, and LiT species, respectively, and conform well to the spacing of the ground and the first excited vibrational states, Table S5. The associated zero-point energies derived from the harmonic oscillator model are ~ 5.9, ~ 4.3, and ~ 3.5 kcal mol^{-1} for LiH, LiD, and LiT species, respectively, and are indeed comparable with the above presented nuclear energy contributions to the hydrogen basins (Theoretically, the zero-point energy of a system may be evaluated by subtracting total non-BO energy from total electronic energy at equilibrium geometry within the CNM neglecting non-adiabatic contributions. But in practice [55], this approach is not accurate enough even in state of art calculations). It is timely to emphasize that the orthodox QTAIM is unable to evaluate the energy contribution of nuclear vibrations to the atomic basin energies [44–46].

The variation of atomic charges in the LiX ($X = H, D, T$) systems, $Q(Li) = 3 - N_-(\Omega)$ and $Q(X) = N_+(\Omega) - N_-(\Omega)$, is less pronounced though observable (~ 0.004 from LiH to LiH(∞)); charge separation gets larger by the increase in the mass of the quantum nuclei. It is tempting to claim based on this observation that the electronegativities of hydrogen isotopes are slightly different, larger for more massive nuclei. Indeed, in their state of art non-BO calculations [23, 24, 56], Adamowicz and coworkers have demonstrated explicitly that in HD^+, HT^+, and HD species electrons are more attracted toward the heavier nucleus. This interpretation is also confirmed by recent computational study of Reyes and coworkers as well as Strasbuger's analysis of HD^+ and HD by his proposed modified adiabatic method [57, 58].

The total electric dipole moments and their basin decomposition, $\vec{d} = \sum_\Omega \vec{d}(\Omega)$, offer a more detailed picture of the electronic and nuclear distributions. Accordingly, assuming the clamped Li nucleus as the center of "global" coordinate system [42], each basin contribution is the summation of the electronic and nuclear contributions, $\vec{d}(\Omega) = \vec{d}_-(\Omega) + \vec{d}_+(\Omega)$, whereas these contributions are decomposed themselves to charge transfer (CT) and polarization (P) contributions (the latter is also called "first moment") [44–46], $\vec{d}_\pm(\Omega) = \vec{d}_\pm^{CT}(\Omega) + \vec{d}_\pm^{P}(\Omega)$ [42]. Table 2 presents all these contributions for the considered systems taking the (3, −3) CPs of ρ_+ and Γ as the center of "local" coordinate systems to describe $\vec{d}_+(\Omega)$ and

$\vec{d}_-(\Omega)$ of the hydrogen basins, respectively [42]. It is evident from this table that the total electric dipole moments are slightly different in these systems and are slightly larger for species containing heavier nucleus. Since the single s-type spherical Gaussian function used as nuclear basis function is located just at (3, −3) CP of ρ_+, the P dipole of $\vec{d}_+(\Omega)$ is null and quantum nuclei participate in electric dipole moments only by their CT dipole moments; the latter is also null in the Li basin since the nuclear distribution is confined to the hydrogen atomic basin demonstrating that $\vec{d}_+ = \vec{d}_+^{CT}(X)$; $(X = H, D, T)$, $(\vec{d}_+(Li) = 0)$. The CT dipole, $\vec{d}_+^{CT}(X) = N_X(\Omega) \times \langle R_{Li-X} \rangle = \langle R_{Li-X} \rangle$, is smaller for heavier species due to the fact that the mean Li-X distance, $\langle R_{Li-X} \rangle$, is smaller for heavier species, Tables S1–S3. On the other hand, the electronic P dipole contribution for Li basin is very small and relatively constant demonstrating the fact that the electronic distribution is almost spherical in this basin, whereas CT dipole contribution is null since the origin of local coordinate system of this basin is placed on the Li nucleus; thus, $\vec{d}_-(Li) \approx 0$. One may sum up all these and claim that $\vec{d}(LiX) \approx \vec{d}_-^P(X) + \vec{d}_-^{CT}(X) + \vec{d}_+^{CT}(X) = \vec{d}_-^P(X) + \vec{d}^{CT}(X)$. It is interesting to note that in contrast to previously mentioned electronegativity trend, since the (3, −3) CP of Γ tends toward Li nucleus in heavier species, the electronic CT dipoles like nuclear CT dipoles diminish in heavier species.

Therefore, without taking the contribution of $\vec{d}_-^P(X)$ into account, the observed trend for the variation of total dipole moments with nuclear mass is *not* reproducible. This observation is a clear sign that the amount of charge separation, as discussed previously, is *not* the exclusive origin of the observed trend of total dipole moments and the polarization of electronic distribution of the hydrogen basin has also a key role, containing the fingerprint of nuclear mass.

3.3 Vibrational excitations

In order to reveal the role of nuclear vibrational excitations on the AIM analysis, the [6s:1p$_z$] wavefunctions were considered, Table S7. It is evident from the relief and contour maps in Figs. 3 and S3 that ρ_+ now contains a single node as one expects from the first excited vibrational state; however, the general structure and topological characteristics of ρ_- are similar to that observed for the previously considered ground state wavefunctions, Fig. 1. From the topological analysis of Γ, peculiar pattern emerges namely three instead of one CP in the hydrogen basin, Fig. 3; a detailed consideration of Γ reveals the fact that this field has two local maxima in hydrogen basin instead of one, Fig. S4, demonstrating the non-negligible

Fig. 3 A typical relief map (*top*) of $\rho+$ for the considered system calculated at FV-MC-MO/[6s:1p$_z$] level. The Li clamped nucleus is located at (0,0) point. A typical molecular graph (*bottom*) of Γ at the same computational level; the *pink dots* are (3, −3) CPs, whereas *red dots* are (3, −1) CPs. The clamped Li nucleus is located very near to the *pink dot* in the *left-hand side*
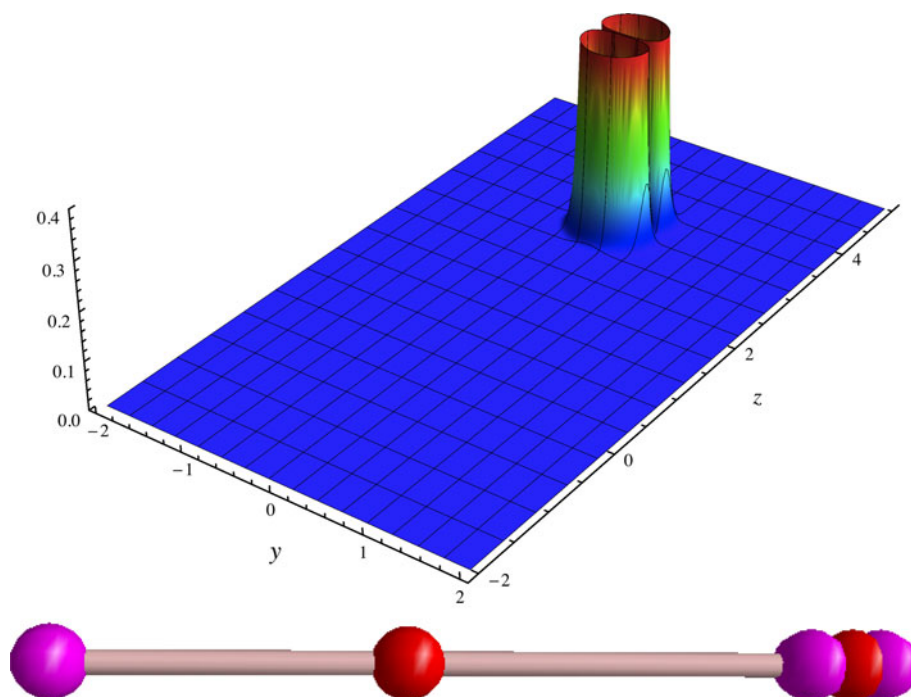
role of nuclear vibrational excitations on the AIM analysis. Accordingly, one may claim that in this quantum state, hydrogen atom is divided into two basins each containing a (3, −3) CP separated by a zero-flux surface going through the (3, −1) CP. For uniformity, in this contribution, the sum of these basins is considered as a single atomic basin but to emphasize their peculiarity, these are called as *united* hydrogen basins (It is interesting to note that based on a heuristic but ad hoc approach the emergence of such features due to nuclear dynamics were predicted by Cassam-chenaï and Jayatilaka [59]; however, since authors did not consistently formulated an AIM method for excited vibrational states, this and similar proposals remained tentative and generally were not well received. Also, the AIM approach proposed in this study somehow bypasses the obstacles put forward by them that originate from inconsistent incorporation of nuclear dynamics within the context of the orthodox QTAIM).

Table 3 presents the results of topological analysis of Γ, ρ_-, and ρ_+ in the three considered systems. Numerous similarities are evident when one compares these results with those offered in Table 1 for the ground state; the similar trends are not reiterated here. However, once again a detailed inspection reveals delicate differences and demonstrates that the change of nuclear vibrational state reflects itself even on the topological indexes at the BCP of Γ. Particularly, the position of the BCP and thus the interatomic boundary relative to the Li nucleus is different from those offered in Table 1; for each species, it is located at a slightly more distant position from Li nucleus relative to that derived from the analysis of the ground state Γ.

A detailed consideration of nuclear distribution demonstrates that ESDs in this state are almost the same with those of ground state, Table S8; thus, the differences of indexes at BCPs for ground and excited states are exclusively due to varied polarization of electrons, ρ_-, in the presence of excited nuclear distribution, ρ_+. In other words, one may reemphasize that the change of nuclear distribution marks its fingerprint on electronic distribution.

Table 4 presents some properties of the lithium and united hydrogen basins. It is evident from this table that the amount of the net flux integral of each atomic basin is quite low and the summation of basin energies and electric dipole moments conform well to the total ab initio calculated values, Table S9. Most trends in this set of basin properties are similar to that observed and described for the ground states of the considered species so there are not restated here. A comparison with Table 2 demonstrates that the amount and also the relative importance of the nuclear energy contributions in total energies of the united hydrogen basins are larger for this state revealing the expected effect of vibrational excitations. The charge separations are slightly smaller than the ground state basins; however, both the electronic and nuclear *CT* dipole moments of the united hydrogen basins are larger than those derived for the grounds state hydrogen basins; this is in line with the fact that mean Li-X distance is larger for the excited vibrational states, Table S7. Also, the *P* electronic dipoles of both basins in all species are slightly larger than the ground state values revealing the fact that electronic charge distribution is perturbed in a more *anisotropic* manner than the ground state; this is the expected trend since the nuclear distribution in this

Table 3 The results of topological analysis performed on the LiH, LiD, LiT systems using [6s:1p$_z$] basis set

Property	Γ					ρ$_+$			ρ$_-$		
	Li	BCP	(3, −3)	(3, −1)	(3, −3)	(3, −3)	Midpoint[a]	(3, −3)	Li	BCP	(3, −3)
LiH											
Am. field	11.439	0.026	0.161	0.146	0.152	25.191	0.000	25.191	11.439	0.026	0.148
Lap. field	−3,528.526	0.138	−4.626	1.416	−4.271	−6,675.489	4,536.465	−6,675.489	−3,528.526	0.138	−0.940
Hess. com.	−1,176.177	−0.031	−1.212	−0.328	−1.121	−1,668.872	0.000	−1,668.872	−1,176.177	−0.031	−0.314
	−1,176.172	0.201	−2.201	2.071	−2.030	−3,337.744	4,536.465	−3,337.744	−1,176.172	0.201	−0.312
Dis. (3, −3)[b]	0.000	1.409	3.091	3.268	3.390	3.080	3.253	3.427	0.000	1.409	3.157
G	0.001	0.031	0.004	0.607	0.052	0.000	1,134.116	0.000	0.001	0.031	0.000
K	882.133	−0.004	1.161	0.253	1.120	1,668.872	0.000	1,668.872	882.133	−0.004	0.235
V	−882.134	−0.027	−1.165	−0.859	−1.173	−1,668.872	−1,134.116	−1,668.872	−882.134	−0.027	−0.235
LiD											
Am. field	11.437	0.027	0.170	0.157	0.163	45.181	0.000	45.181	11.437	0.027	0.159
Lap. field	−3,524.913	0.142	−5.959	2.059	−5.611	−17,674.515	12,011.078	−17,674.515	−3,524.913	0.142	−1.077
Hess. com.	−1,174.972	−0.032	−1.555	−0.376	−1.453	−4,418.629	0.000	−4,418.629	−1,174.972	−0.032	−0.360
	−1,174.968	0.207	−2.849	2.811	−2.706	−8,837.257	12,011.078	−8,837.257	−1,174.968	0.207	−0.358
Dis. (3, −3)[b]	0.000	1.403	3.086	3.233	3.337	3.079	3.222	3.365	0.000	1.403	3.135
G	0.001	0.032	0.003	0.805	0.057	0.000	3,002.770	0.000	0.001	0.032	0.000
K	881.229	−0.004	1.493	0.290	1.460	4,418.629	0.000	4,418.629	881.229	−0.004	0.269
V	−881.231	−0.028	−1.496	−1.095	−1.518	−4,418.629	−3,002.770	−4,418.629	−881.231	−0.028	−0.269
LiT											
Am. field	11.436	0.027	0.175	0.162	0.168	62.977	0.000	62.977	11.436	0.027	0.164
Lap. field	−3,523.387	0.144	−6.811	2.506	−6.479	−30,740.817	20,890.551	−30,740.817	−3,523.387	0.144	−1.145
Hess. com.	−1,174.464	−0.033	−1.774	−0.400	−1.666	−7,685.204	20,890.551	−7,685.204	−1,174.464	−0.033	−0.383
	−1,174.459	0.209	−3.263	3.306	−3.147	−15,370.408	0.000	−15,370.408	−1,174.459	0.209	−0.380
Dis. (3, −3)[b]	0.000	1.400	3.085	3.218	3.312	3.080	3.208	3.336	0.000	1.400	3.125
G	0.001	0.032	0.003	0.936	0.060	0.000	5,222.638	0.000	0.001	0.032	0.000
K	880.848	−0.004	1.705	0.309	1.679	7,685.204	0.000	7,685.204	880.848	−0.004	0.286
V	−880.849	−0.028	−1.708	−1.245	−1.739	−7,685.204	−5,222.638	−7,685.204	−880.849	−0.028	−0.286

Field entry denotes the amount of Γ, ρ$_-$ fields, whereas Lap. is an abbreviation for the Laplacian operator. Hess. Com. are the three components of the diagonalized Hessian matrix. The first entry in each case is the degenerate component of the Hessian matrix. dis. is the acronym of "distance from". The *G, K,* and *V* are used to denote the Lagrangian, Hamiltonian, and total virial fields. See references [41] and [42] for details and definitions. All values are presented in the atomic units

[a] Since the two components of the Hessian matrix are zero, the midpoint is best described as a (1, +1) CP. See reference [44] for details

[b] Distance from the (3, −3) CP located very near to Li nucleus

state in contrast to ground vibrational state is quite anisotropic, Fig. 3. Consequently, the total electronic and nuclear electric dipole moments for each basin in comparison with that of ground state congeners are larger, once gain revealing the direct contribution of ρ$_+$ in basin properties as well as its fingerprint on basin properties derived from ρ$_-$.

4 Conclusion and future prospects

This contribution provided the first AIM analysis of a non-BO wavefunction. Since the whole formalism of the TC-QTAIM reduces to the orthodox QTAIM when electrons are the only quantum particles of a molecular system

[43], the present analysis demonstrates that a single unified formalism is capable of extracting *chemical entities*, e.g., atoms in molecules and bonding indexes, from a diverse set of wavefunctions, produced within and beyond the CNM. Accordingly, this formalism is capable of distinguishing atomic basins containing different isotopes thus going beyond the orthodox QTAIM, which is only sensitive to nuclear charge, by incorporating the effect of nuclear mass. In addition, this methodology incorporates nuclear vibrational dynamics from the outset, working with non-Born–Oppenheimer wavefunctions that take nuclear dynamics into account, so it is an efficient tool to study the role of nuclear dynamics on the AIM analysis. Particularly, this formalism is not confined to ground state nuclear

Table 4 The results of the basin integrations performed on LiH, LiD, LiT systems using [6s:1p$_z$] basis set

Molecule/property LiH	Atoms			Molecule/property LiD	Atoms		
	Li	X	Sum		Li	X	Sum
Energy	−7.34253	−0.55222	−7.89474	Energy	−7.34256	−0.56567	−7.90823
Electronic charge	0.91154	−0.91154	0.00000	Electronic charge	0.91342	−0.91342	0.00000
Kinetic energy (G)	7.34251	0.55221	7.89472	Kinetic energy (G)	7.34258	0.56567	7.90825
Kinetic energy (K)	7.34251	0.55222	7.89473	Kinetic energy (K)	7.34258	0.56568	7.90825
Total virial (V)	−14.68505	−1.10444	−15.78949	Total virial (V)	−14.68511	−1.09805	−15.78316
Net flux int.	0.000003	0.000005	–	Net flux int.	0.000002	0.000005	–
Ele. energy	−7.34253	−0.52967	−7.87219	Ele. energy	−7.34256	−0.54902	−7.89158
Nuc. energy	0.00000	−0.02255	−0.02255	Nuc. energy	0.00000	−0.01665	−0.01665
CT ele. dipole[a]	0.00000	−6.21889	−6.21889	CT ele. dipole[a]	0.00000	−6.16468	−6.16468
CT nuc. dipole[a]	0.00000	3.25334	3.25334	CT nuc. dipole[a]	0.00000	3.22181	3.22181
First ele. moment[a]	0.00477	0.49318	0.49795	First ele. moment[a]	0.00327	0.46891	0.47218
First nuc. moment[a]	0.00000	0.00000	0.00000	First nuc. moment[a]	0.00000	0.00000	0.00000
Total ele. dipole	0.00477	−5.72572	−5.72095	Total ele. dipole	0.00327	−5.69577	−5.69250
Total nuc. dipole	0.00000	3.25334	3.25334	Total nuc. dipole	0.00000	3.22181	3.22181
Total dipole	0.00477	−2.47237	−2.46760	Total dipole	0.00327	−2.47396	−2.47070

LiT	Li	X	Sum
Energy	−7.34261	−0.57177	−7.91438
Electronic charge	0.91425	−0.91425	0.00000
Kinetic energy (G)	7.34261	0.57177	7.91438
Kinetic energy (K)	7.34261	0.57177	7.91438
Total virial (V)	−14.68521	−1.14355	−15.82876
Net flux int.	0.000003	0.000005	–
Ele. energy	−7.34261	−0.55790	−7.90051
Nuc. energy	0.00000	−0.01387	−0.01387
CT ele. dipole[a]	0.00000	−6.14083	−6.14083
CT nuc. dipole[a]	0.00000	3.20796	3.20796
First ele. moment[a]	0.00265	0.45853	0.46119
First nuc. moment[a]	0.00000	0.00000	0.00000
Total ele. dipole	0.00265	−5.68230	−5.67965
Total nuc. dipole	0.00000	3.20796	3.20796
Total dipole	0.00265	−2.47434	−2.47169

The int., ele., and nuc. are abbreviations for integral, electronic, and nuclear, respectively. See references [41] and [42] for details and definitions. All values are presented in the atomic units

[a] The local center of coordinate system for each basin is the position of lithium nucleus and the position of $(1, +1)$ CP of ρ_+ (denoted as "midpoint" in Table 3) for the lithium and hydrogen basins, respectively

wavefunctions, and excited nuclear vibrational states are also treatable in this framework. This capability sets the stage to conceive a general AIM approach that takes all nuclear excursions, not only the vibrations of lightest nuclei, into account.

On the other hand, the presented numerical results demonstrate that although the direct nuclear contributions to the topological indexes are generally negligible at the BCPs, a fact that is probably extendable to heavier nuclei because of their more localized nuclear distributions and

smaller ESDs, its contribution to basin properties is appreciable and quite beyond the chemical accuracy; indirect effects of quantum nucleus distribution on the electron density also prompted delicate differences in both topological indexes and basin properties of isotopomers. One expects that for heavier nuclei, all such effects diminish and for sufficiently large nuclear masses, both direct and indirect contributions eventually disappear, and numerical results of the presented AIM analysis tend toward the orthodox QTAIM results that are derived within

the CNM. In other words, in the high mass limit, one expects that TC-QTAIM analysis to be virtually indistinguishable from the orthodox QTAIM. This issue will be considered in detail in a forthcoming contribution.

Whereas in this study only systems containing a single quantum nucleus were considered in computational studies, the TC-QTAIM is capable of dealing with multiproton or multideuteron systems as well. In future computational studies, such targets are worth of consideration. Also, a *multicomponent* version of the presented AIM methodology that may be called as multicomponent quantum theory of atoms in molecules (MC-QTAIM) is desirable to be formulated in order to consider systems with two or more types of quantum nuclei; molecules containing both protons and deuterons are clear examples. These issues are all under scrutinization in our laboratory, and the final results will be offered in future publications.

References

1. Born M, Oppenheimer JR (1927) Ann Phys (Leipzig) 84:457
2. Baer M (2006) Beyond born-oppenhiemer. Wiley-Interscience, New Jersey
3. Sutcliffe BT, Woolley RG (2005) Phys Chem Chem Phys 7:3664
4. Sutcliffe BT (1996) Int J Quantum Chem 58:645
5. Woolley RG (1991) J Mol Struc (Theochem) 230:17
6. Primas H (1983) Chemistry, quantum mechanics and reductionism. Springer, Berlin
7. Tapia O (2006) J Math Chem 39:637
8. Monkhorst HJ (1999) Int J Quantum Chem 72:281
9. Udagawa T, Tachikawa M (2009) Multi-component molecular orbital theory. Nova Science Publishers, New York
10. Ishimoto T, Tachikawa M, Nagashima U (2009) Int J Quantum Chem 109:2677
11. Kreibich T, Leeuwen RV, Gross EKU (2008) Phys Rev A 78:022501
12. Nakai H (2007) Int J Quantum Chem 107:2849
13. Bubin S, Cafiero M, Adamowicz L (2005) Adv Chem Phys 131:377
14. Bochevarov AD, Valeev EF, Sherrill CD (2004) Mol Phys 102:111
15. Harris FE (2004) Adv Quantum Chem 47:129
16. Cafiero M, Bubin S, Adamowicz L (2003) Phys Chem Chem Phys 5:1491
17. Kozlowski PM, Adamowicz L (1993) Chem Rev 93:2007
18. Auer B, Pak MV, Hammes-Schiffer S (2010) J Phys Chem C 114:5582
19. Hilikata Y, Nakashima H, Nakatsuji H (2009) J Chem Phys 130:024102
20. Rebane TK (2010) Opt Spect 109:66
21. Cafiero M, Adamowicz L (2002) Phys Rev Lett 88:033002
22. Cafiero M, Adamowicz L (2002) Phys Rev Lett 89:073001
23. Bubin S, Bednarz E, Adamowicz L (2005) J Chem Phys 122:041102
24. Bednarz E, Bubin S, Adamowicz L (2005) J Chem Phys 122:164302
25. Hammes-Schiffer S (2002) Chem Phys Chem 3:33
26. Swalina C, Pak MV, Chakraborty A, Hammes-Schiffer S (2006) J Phys Chem A 110:9983
27. Pak MV, Hammes-Schiffer S (2004) Phys Rev Lett 92:103002
28. Tachikawa M, Ishimoto T, Tokiwa H, Kasatani H, Deguchi K (2002) Ferroelectrics 268:3
29. Tachikawa M (2002) Mol Phys 100:881
30. Ishimoto T, Tachikawa M, Yamauchi M, Kitagawa H, Tokiwa H, Nagashima U (2003) Chem Phys Lett 372:503
31. Udagawa T, Ishimoto T, Tokiwa H, Tachikawa M, Nagashima U (2003) Chem Phys Lett 389:236
32. Shibl MF, Tachikawa M, Kühn O (2005) Phys Chem Chem Phys 7:1368
33. Udagawa T, Ishimoto T, Tokiwa H, Tachikawa M, Nagashima U (2006) J Phys Chem A 110:7279
34. Itou Y, Mori S, Udagawa T, Tachikawa M, Ishimoto T, Nagashima U (2007) J Phys Chem A 111:261
35. Ishimoto T, Ishihara Y, Teramae H, Baba M, Nagashima U (2008) J Chem Phys 128:184309
36. González SA, Aguirre NF, Reyes A (2008) Int J Quantum Chem 108:1742
37. Kikuta Y, Ishimoto T, Nagashima U (2008) Chem Phys 354:218
38. Swalina C, Wang Q, Chakraborty A, Hammes-Schiffer S (2007) J Phys Chem A 111:2206
39. Cafiero M, Adamowicz L (2004) Chem Phys Lett 387:136
40. Cafiero M, Adamowicz L (2007) Int J Quantum Chem 107:2679
41. Nasertayoob P, Goli M, Shahbazian Sh (2011) Int J Quantum Chem. doi:10.1002/qua.22495
42. Goli M, Shahbazian Sh (2011) Int J Quantum Chem. doi:10.1002/qua.22805
43. Zadeh FH, Shahbazian Sh (2011) Int J Quantum Chem. doi:10.1002/qua.22881
44. Bader RWF (1990) Atoms in molecules: a quantum theory. Oxford University Press, Oxford
45. Popelier PLA (2000) Atoms in molecules an introduction. Pearson, London
46. Matta C, Boyd RJ (2007) Quantum theory of atoms in molecules: from solid state to DNA and drug design. Wiley-VCH, Weinheim
47. Anderson JSM, Ayers PW, Rodriguez Hernandez JI (2010) J Phys Chem A 114:8884
48. Cohen L (1979) J Chem Phys 70:788
49. Cohen L (1984) J Chem Phys 80:4277
50. Biegler-König F (2000) J Comput Chem 21:1040
51. Biegler-König F, Schönbohm J, Bayles D (2001) J Comput Chem 22:545
52. Biegler-König F, Schönbohm J (2002) J Comput Chem 23:1489
53. Tachikawa M, Mori K, Suzuki K, Iguchi K (1998) Int J Quantum Chem 70:491
54. Tachikawa M, Mori K, Nakai H, Iguchi K (1998) Chem Phys Lett 290:437
55. Scheu CE, Kinghorn DB, Adamowicz L (2001) J Chem Phys 114:3393
56. Bubin S, Leonarski F, Stanke M, Adamowicz L (2009) J Chem Phys 130:124120
57. Moreno DV, González SA, Reyes A (2010) J Phys Chem A 114:9231
58. Strasburger K (2009) J Chem Phys 131:134103
59. Cassam-chenaï P, Jayatilaka D (2001) Theor Chem Acc 105:213